

A CFD STUDY OF SQUARE PIN FINS AIR-COOLED HEAT SINKS

Flávia Milo dos Santos, milo@ita.br

Edson Luiz Zapparoli, zapparoli@ita.br

Cláudia Regina de Andrade, claudia@ita.br

Instituto Tecnológico de Aeronáutica, Departamento de Engenharia Aeronáutica e Mecânica, Área de Aerodinâmica, Propulsão e Energia - Praça Marechal Eduardo Gomes, 50, Vila das Acácias, CEP 12.228-900, São José dos Campos, SP, Brasil.

Abstract. Nowadays, finned air-cooled heat sinks are still the most popular means for electronic equipment cooling. Passive heat sinks are cooled by air natural convection while in the active dissipators the heat is transferred to a forced convection fan induced air flow. The decrease of the heat dissipation capacity due to the reduction in the heat exchange area represents a restriction in the evolution of the electronic components compactness. Hence, researches must be carried out to improve the heat transfer processes simulation and to increase the heat sinks effectiveness. At the present work, the Reynolds Averaged Navier-Stokes (mass, momentum and energy) and $k-\epsilon$ turbulence model equations are numerically solved employing the finite volume method and a segregated velocity-pressure coupling to analyze the square pin fins air-cooled heat sinks in a staggered arrangement. A mesh sensitivity study and a comparison with experimental results were performed to validate the numerical procedure. Pressure drop and heat transfer coefficient were obtained to evaluate the heat sink performance as a function of the frontal velocity.

Keywords: pin fin, heat sink, CFD, electronic cooling

1. INTRODUCTION

With the continuous rise in the electronic equipments performance, followed by an increases in the powerful and components compactness, the removal of the high heat fluxes becomes an important factor to maintain the working temperature of equipments below certain threshold temperature.

Passive heat sinks are cooled by air natural convection while in the active (direct air-cooling) dissipators the heat is transferred to a forced convection fan induced air flow. Direct air-cooling is still the most popular means for cooling of electronics because of low cost and high reliability and efficiency. To enhance the thermal performance, are usually used finned surfaces to increase the heat transfer rate for a given heat sink area. Hence, extensive studies have been made of heat transfer and flow characteristics of various configurations of finned heat sinks.

Dogruoz (2005) presented experimental and modeling study of the hydraulic resistance and heat transfer of square pin fin heat sink with inline arrangement and obtained that the agreement between the theoretical and experimental temperature results decay when the approach velocities and heat sink decrease.

Mohamed (2006) performed experimental investigations of the heat transfer characteristics of heat sinks with various square modules array and inline arrangement and examined the effects of flowing air velocity, base temperature of modules array and module to channel height ratio. The results demonstrated that the average heat transfer coefficient increases slightly with increasing the modules array base temperature and increases significantly with increasing the flowing air velocities.

Sahiti *et al.* (2006) studied numerically the form how the pin fin cross-section (NACA, dropform, lancet, elliptic, circular and square) influences the pressure drop and heat transfer performance by testing inline and staggered arrangements. This investigation indicated that NACA profile presents little advantage over the others studied configurations.

Yang *et al.* (2007a) conducted a series of experiments to examine the thermal hydraulic performance of heat sinks having plate, slit and louver fin patterns. It was concluded that heat transfer coefficients and the pressure drop increase with the rise of frontal velocity and the louver fin usually presents better heat transfer performance and higher pressure drops than the slit fin pattern. They found also a significant drop of heat transfer performance at a low Reynolds number and at small fin spacing. Experiments of Yang *et al.* (2007b) examined the effect of fin density on the heat transfer performance and pressure drop for pin fin heat sinks having circular, elliptic and square cross-section, with inline and staggered arrangement. It was noticed that the heat transfer coefficient and the pressure drop increase with the rise of frontal velocity. The results demonstrated that the inline arrangement presented a significant effect of fin density on the heat transfer coefficient of circular pin fin and small effect for an elliptic fin, except when the frontal velocity was above 3 m/s. This effect was no significant for square fin geometry. For the staggered arrangement, all configurations presented rise in the heat transfer coefficient with the increase of the fin density. According to these authors, the elliptic pin fin showed the lowest pressure drop.

At this context, the present work focuses on a numerical study based on the experimental conditions of Yang *et al.* (2007b). The mathematical model (continuity, momentum, energy and realizable $k-\epsilon$ turbulence model) was solved using the finite volume method, in order to investigate the pin fin heat sink dissipator performance under air forced convection, analyzing the influence of the frontal velocity on the heat transfer coefficient and pressure drop results.

2. PROBLEM DEFINITION

The 3-D conjugate heat transfer in an air-cooled heat sink will be solved using a CFD tool. At this procedure, a computational domain is constructed in accordance to the experimental setup of Yang *et al.* (2007b). Figure 1 shows the heat sink isometric view, showing solid region and fluid flow domains with 25 pins. Opaques surfaces in Fig. 1 represent the internal interface between the pin fin heat sink and the air. The transparent body symbolizes the border of simulate region, in which the air flows. In this transparent region the walls are represented by non-slip wall and adiabatic wall boundary conditions, except by the inlet and outlet surfaces.

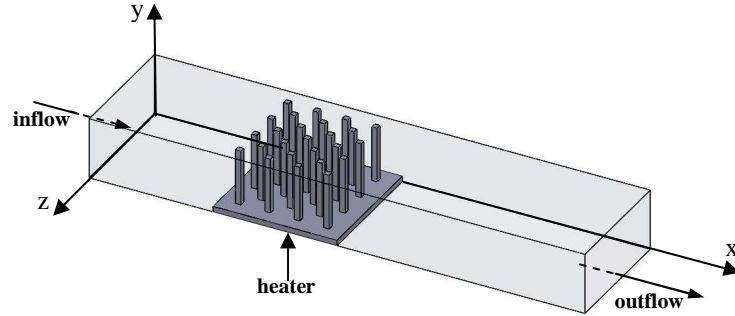


Figure 1. Computational domain

The uniform heat flux is applied at the bottom heat sink surface (dissipator underneath surface). The heat is removed of the heat sink by conduction, from the heat sink base until the extended surfaces top (pin fin) and by convective heat transfer to the environment. In the interface, the coupling between convective and conductive heat transfer is represented by temperatures and heat flux equalities, non-slip wall boundary conditions to airflow and wall law for turbulent variables. Geometric parameters of the computational domain are showed in Fig. 2 and their dimensions are presented in Tab. 1.

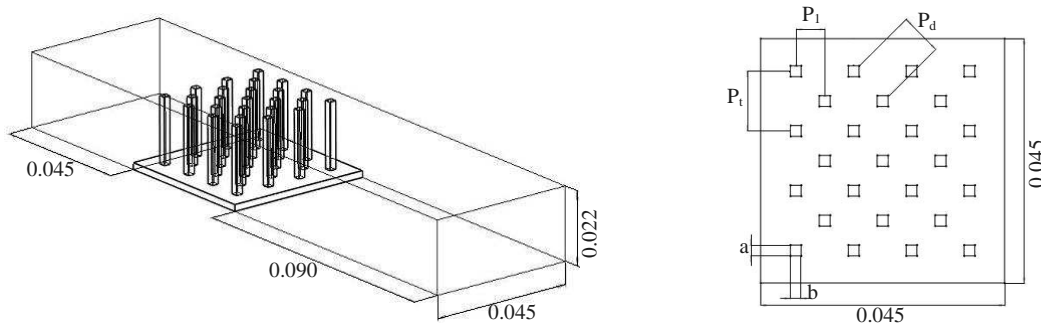


Figure 2. Geometric parameters of the pin fin heat sink (dimensions in m)

The heat sink material used in the present investigation is aluminium alloy, with thermal conductivity equal to 170 W/(m·K). A constant heat rate of 25 W is applied through a 45 mm · 45 mm heating surface in bottom heat sink base surface. The air physical properties are: $\rho = 1.225 \text{ kg/m}^3$, $\mu = 1.7894 \cdot 10^{-5} \text{ kg/(m.s)}$, $C_p = 1006.43 \text{ J/(kg.K)}$, $k = 0.0242 \text{ W/(m.k)}$.

Table 1. Dimensions geometric of the pin fin heat sink.

a (m)	b (m)	Number of fins (N)	P_t (m)	P_1 (m)	P_d (m)
0.002	0.002	25	0.011	0.00534	0.00767

3. MATHEMATICAL MODELING

The governing differential equations system for an incompressible turbulent steady-state conjugate problem with constant solid and fluid properties is described by Eqs. (1) to (6). Natural convection and radiation heat transfer are neglected. The turbulence effects are taken account employing an eddy-viscosity based model (realizable $k - \epsilon$ model) and a non-equilibrium function to evaluate the wall treatment close to solid regions. The used nomenclature is presented in Tab. 2.

Continuity and momentum equations

$$\frac{\partial}{\partial x_i}(\rho u_i) = 0 \quad (1)$$

$$\frac{\partial}{\partial x_i}(u_i u_j) = -\frac{1}{\rho} \frac{\partial p}{\partial x_j} + \frac{1}{\rho} \frac{\partial}{\partial x_i}(\tau_{ij}) \quad (2)$$

Energy equation

$$\frac{\partial(\rho u_i T)}{\partial x_i} = \frac{\partial}{\partial x_i} \left(\Gamma_E \frac{\partial T}{\partial x_i} \right) \quad (3)$$

In the solid domain, Eq. (3) is simplified to:

$$\frac{\partial}{\partial x_i} \left(\Gamma_s \frac{\partial T}{\partial x_i} \right) = 0 \quad (4)$$

Equations of the realizable k-ε model

After Shih *et al.* (1995), the realizable k-ε model equations are:

$$\frac{\partial}{\partial x_i}(\rho k u_i) = \frac{\partial}{\partial x_i} \left[\left(\mu + \frac{\mu_t}{\sigma_k} \right) \frac{\partial k}{\partial x_i} \right] + G_k - \rho \epsilon \quad (5)$$

$$\frac{\partial}{\partial x_i}(\rho \epsilon u_i) = \frac{\partial}{\partial x_i} \left[\left(\mu + \frac{\mu_t}{\sigma_\epsilon} \right) \frac{\partial \epsilon}{\partial x_i} \right] + \rho C_1 S \epsilon - \rho C_2 \frac{\epsilon^2}{k + \sqrt{v \epsilon}} \quad (6)$$

where

$$C_1 = \max \left[0.43, \frac{\eta}{\eta + 5} \right]; \quad \eta = S \frac{k}{\epsilon}; \quad S = \sqrt{2 S_{ij} S_{ij}} \quad (7)$$

The constant values of the realizable k - ε model used in this work are: $C_2=1.9$; $\sigma_k=1.0$; $\sigma_\epsilon=1.2$.
The eddy viscosity is computed from:

$$\mu_t = \rho C_\mu \frac{k^2}{\epsilon} \quad (8)$$

where C_μ is no longer constant as in the standard k-ε model. In this model, C_μ is calculated as follows:

$$C_\mu = \frac{1}{A_0 + A_S \frac{k U^*}{\epsilon}}; \quad U^* \equiv \tilde{S} = \sqrt{S_{ij} S_{ij}}; \quad A_0 = 4.04; \quad A_S = \sqrt{6} \cos \phi; \quad \phi = \frac{1}{3} \cos^{-1}(\sqrt{6} W); \quad W = \frac{S_{ij} S_{jk} S_{ki}}{\tilde{S}} \quad (9)$$

Non-equilibrium wall function

The non-equilibrium wall function was developed under two-layer-based concept by Kim and Choudhury (1995) in order to compute the budget of turbulence kinetic energy in the wall-neighboring cells. The log-law for mean velocity considering the pressure gradient effects yields:

$$\frac{\tilde{U} C_\mu^{1/4} k_p^{1/2}}{\tau_w / \rho} = \frac{1}{\kappa} \ln \left(E \frac{\rho C_\mu^{1/4} k_p^{1/2} y_p}{\mu} \right); \quad \tilde{U} = U - \frac{1}{2} \frac{dp}{dx} \left[\frac{y_v}{\rho \kappa \sqrt{k}} \ln \left(\frac{y}{y_v} \right) + \frac{y - y_v}{\rho \kappa \sqrt{k}} + \frac{y_v^2}{\mu} \right] \quad (10)$$

and y_v is the physical viscous sublayer thickness, and is computed from:

$$y_v = \frac{\mu y_v^*}{\rho C_\mu^{1/4} k_p^{1/2}} \quad (11)$$

where $y_v^* = 11.225$.

The used law-of-the-wall for mean temperature was proposed by Launder and Spalding (1974).

Table 2. Nomenclature.

C_2	constant of the k - ϵ model;
E	empirical constant (=9.793);
G_k	generation of turbulence kinetic energy due to the mean velocity gradients;
k	turbulence kinetic energy;
k_p	turbulence kinetic energy at point P;
p	pressure;
S_{ij}	mean strain rate $\left(S_{ij} = \frac{1}{2} \left(\frac{\partial u_j}{\partial x_i} + \frac{\partial u_i}{\partial x_j} \right) \right)$;
T	temperature;
U^*	mean velocity;
y_p	distance from point P to the wall;
ϵ	dissipation rate;
κ	Von Kármán constant (=0.4187);
μ	molecular dynamic fluid viscosity;
μ_t	turbulent dynamic fluid viscosity;
ν	kinematic viscosity;
ρ	fluid density;
σ_k and σ_ϵ	effective Prandtl numbers for (k) and (ϵ), respectively;
τ_{ij}	stress tensor components $\tau_{ij} = (\mu + \mu_t) \left(\frac{\partial u_j}{\partial x_i} + \frac{\partial u_i}{\partial x_j} \right) - \frac{2}{3} (\mu + \mu_t) \frac{\partial u_l}{\partial x_l} \delta_{ij}$;
Γ_E	effective thermal conductivity $\Gamma_E = \Gamma + \Gamma_T$;
Γ_s	solid thermal conductivity.

Boundary Conditions

Boundary conditions are required for the equations system presented in Eq. (1) to Eq. (6). At the solid domain, only energy equation is solved. In the bottom heat sink surface (dissipator underneath), a constant heat flux is applied. At the solid-fluid interfaces, a continuity temperature and heat flux is guaranteed.

At inflow surface ($x = 0$ m, Fig. 1) a uniform normal velocity and temperature are specified and the transversal velocity components are imposed to be zero as shown in Tab. 3. Non-slip wall and adiabatic boundary conditions are imposed at the duct airflow lateral surfaces. For the turbulence quantities, a turbulence intensity of 5% and viscosity ratio of 10 is specified. The inlet velocity value (V_{in}) is determined according to frontal velocity (V_{fr}) used by Yang *et al* (2007b) and given by:

$$V_{in} = \sigma V_{fr} \quad (12)$$

where σ is the minimum free airflow area (A_{ff}) to total duct area (A_{fr}) ratio.

In the pin fins surfaces is imposed non-slip wall boundary condition for airflow employing wall law and internal interface for heat transfer. Tab. 3 presents the surfaces and used boundary conditions.

Table 3. Surfaces, boundary condition types and boundary conditions.

Surfaces	Boundary condition types	Boundary conditions
Inflow	Inlet	U = uniform, V=W=0, T=298.15 K
Dissipator underneath	Wall	q = 12,345.68 W/m ² (heat flux)
Outflow	Outlet	p = 0; $\frac{\partial U}{\partial n} = \frac{\partial V}{\partial n} = \frac{\partial W}{\partial n} = \frac{\partial T}{\partial n} = 0$
Pin fins	Internal Interface	Non-Slip Wall, non-equilibrium wall function
Lateral surfaces	Wall	Non-Slip Wall, $\frac{\partial T}{\partial n} = 0$ (Adiabatic) non-equilibrium wall function.

The average convection heat transfer coefficient used in all calculations is given by the following expression:

$$h = \frac{\dot{Q}_{conv}}{A_0 \eta_0 \Delta T_{LM}} \quad (13)$$

where \dot{Q}_{conv} is equal to the heat rate imposed in the dissipator underneath surface, A_0 is the total surface area, η_0 is the surface efficiency and ΔT_{LM} is the log mean average temperature, which can be expressed by:

$$\Delta T_{LM} = \frac{(T_w - T_{a,in}) - (T_w - T_{a,out})}{\ln\left(\frac{T_w - T_{a,in}}{T_w - T_{a,out}}\right)} \quad (14)$$

In the Eq. (15), T_w represents the average wall temperature at the dissipator underneath surface, $T_{a,in}$ is the inlet air temperature and $T_{a,out}$ is the outlet air temperature. The surface efficiency is:

$$\eta_0 = 1 - \frac{NA_f}{A_0} (1 - \eta) \quad (15)$$

where η is the fin efficiency and A_0 is the addition of the base surface area (A_b) and of the pin fin surface area (NA_f). The fin efficiency is described by:

$$\eta = \frac{\tanh(mL)}{mL}; \quad m = \sqrt{\frac{hP}{\Gamma_s A_c}} \quad (16)$$

where $L = 0.020$ m (fin length), P represents the fin perimeter and A_c represents the cross-section area of the fin.

It can be noted that an iterative procedure is required to determine the average h value, see Eq. (13) and Eq. (16).

4. COMPUTATIONAL STRATEGY

The numerical simulations have been performed using a CFD commercial code based on finite volume method (FVM), Fluent (2006). The continuity, momentum, energy and $k-\varepsilon$ transport equations for the conjugate problem were solved using steady-state formulation. A successive tetrahedral grid refinement study was performed and mesh information is presented in Tab. 4. These tests showed that the T_{out} values were mesh independent. The finest mesh was chosen to capture the pins fluid flow wakes.

The simulations were performed for $V_{fr} = 1$ m/s to 5 m/s. As a strategy for velocity-pressure coupling, a segregated formulation (SIMPLE algorithm) was utilized. All simulations were carried out until the normalized maximum residuals of the continuity, momentum, energy, k and ε equations decay reaching a value of 10^{-4} , 10^{-4} , 10^{-6} , $5 \cdot 10^{-4}$, respectively.

Table 4. Mesh information, $V_{fr} = 1$ m/s.

Mesh	Cell numbers	T_{out}
1	1,394,650	330.86
2	2,045,623	330.87
3	3,266,236	330.86

5. RESULTS

Numerical results were obtained using a six nodes cluster (AMD Athlon 64 Linux OS) and the total CPU time for finest mesh was 600 min ($V_{fr} = 3$ m/s). The influence of the frontal velocity on the pressure drop (bulk average pressure between duct inlet and outlet surfaces) is shown in Fig. 3, comparing experimental and present work numerical results. There is a better agreement at lower V_{fr} values and the discrepancies intensify for the two higher V_{fr} values simulated.

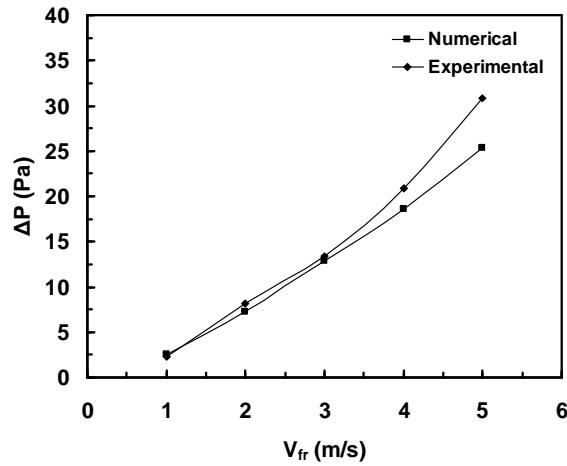


Figure 3. The influence of the frontal velocity on the pressure drop

Figure 4 shows the velocity and thermal wakes for $V_{fr} = 5$ m/s. There is a velocity increase due to pin obstructions. After the first pins row, all pins stay on thermal and velocity wakes that reduces the heat transfer rate as shown by the higher temperatures along the last pins row in Fig. 4b.

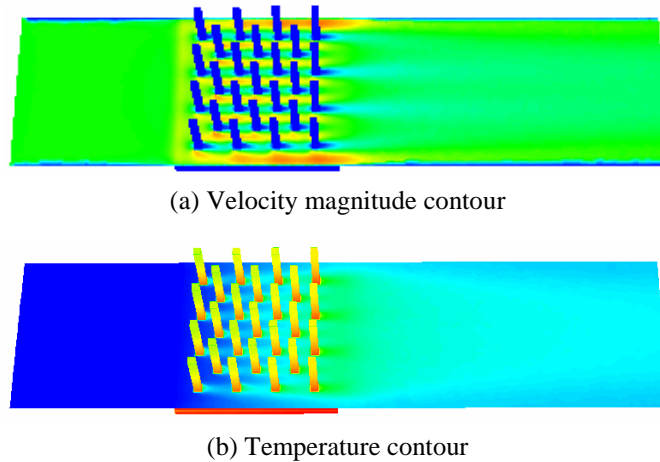


Figure 4. Velocity magnitude and temperature contours at a xz-plane ($y = 0.004$ m). Blue and red colors indicate minimum and maximum values, respectively

Figure 5 shows numerical results for the dissipator and fluid temperature distribution for two frontal velocities. It is observed that the average dissipator temperature decreases when the frontal velocity is higher due to the convection coefficient increase. Besides, the bulk fluid temperature also decays.

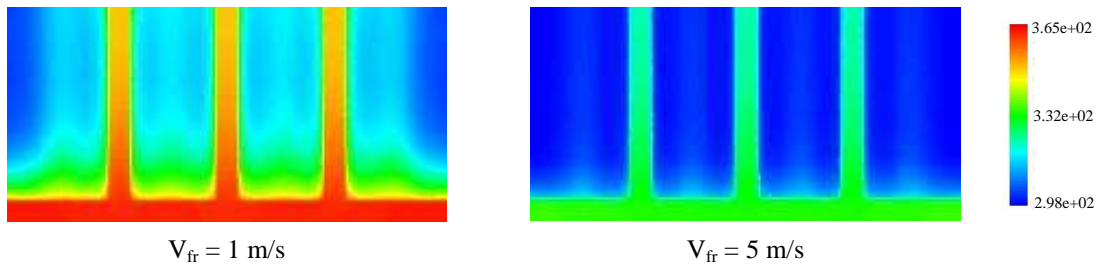


Figure 5. The temperature distribution at the heat sink mid-plane for two frontal velocities

Figure 6 presents the centerline temperature profiles of the central pin of the Fig. 5 for the two above frontal velocities. The dissipator underneath surface temperature at the pin base is higher for $V_{fr} = 1$ m/s (Fig. 6a), but it occurs a larger relative temperature variation inside the dissipator for $V_{fr} = 5$ m/s, determined as a dimensionless temperature shown in Fig. 6b.

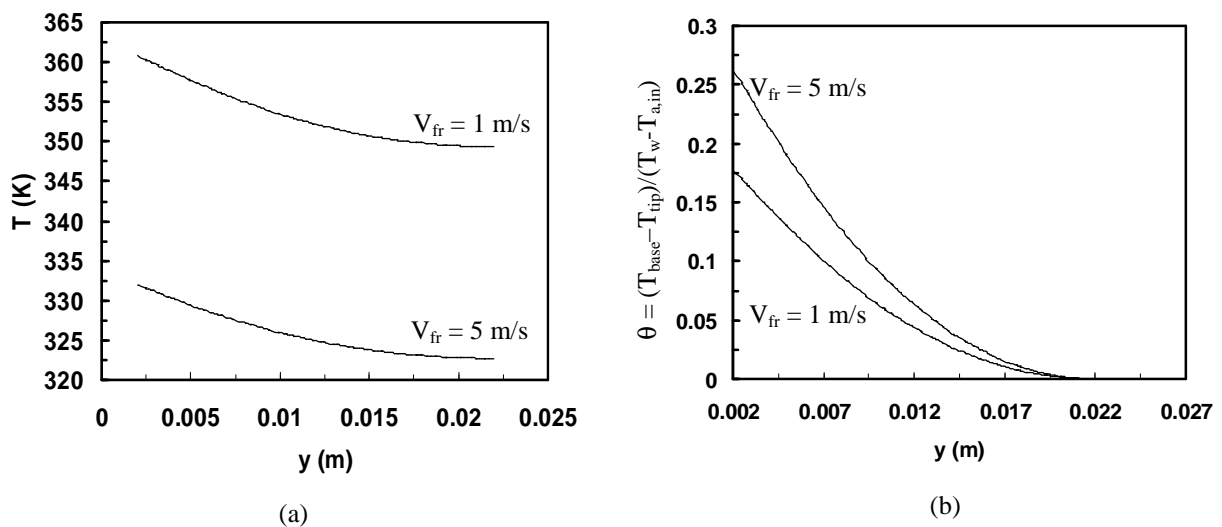


Figure 6. Temperature along the central pin of the dissipator mid-plane: (a) dimensional profile, (b) dimensionless profile

The heat sink performance can be evaluated determining the heat transfer coefficient as depicted in Fig. 7. This coefficient increases more accentuated at lower frontal velocity values that is accompanied by a intense decay in the dissipator underneath surface temperature, Fig. 8. This effect must be carefully observed by the heat sink designer because the present work results showed a few heat transfer rate increase for a considerable pumping power increase requirements when the frontal velocity elevates (saturation level for $V_{fr} > 5$ m/s).

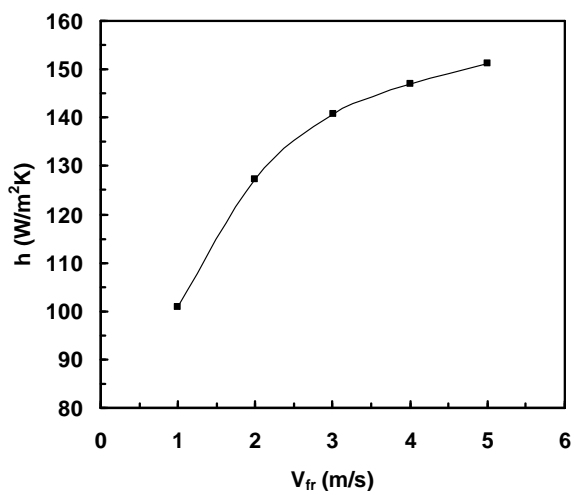


Figure 7. Heat transfer coefficient as a function frontal velocity

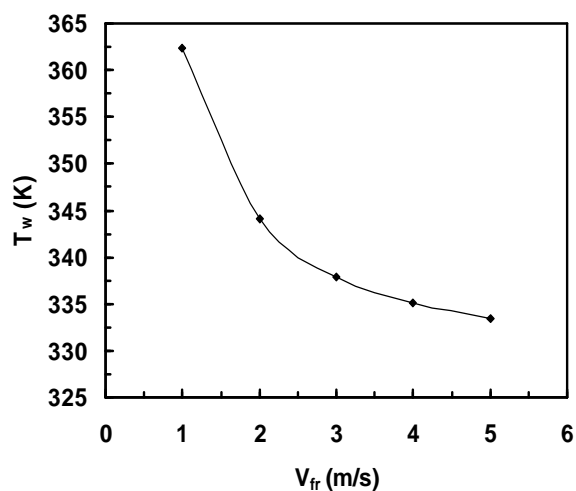


Figure 8. Dissipator underneath surface temperature as a function of frontal velocity

6. FINAL REMARKS

At the present study, a 3-D conjugate heat transfer and fluid flow problem was numerically solved. Temperature and pressure drop results for a heat sink composed by 25 pins staggered arrangement were obtained to determine its performance as a function of the duct inlet frontal velocity. It was concluded that the lower dissipator underneath surface temperature values appeared as frontal velocity increases, resulting in a better heat sink performance. Future works can evaluate other effects on the heat transfer rate: (i) pins arrangement (in-line, e.g); (ii) higher pin fin density and different cross-sections.

7. ACKNOWLEDGEMENTS

The first author would like to acknowledge the CAPES by the financial support and the GSET (Group of Simulation of Flow and Heat Transfer) by the computational support.

8. REFERENCES

- Dogruoz, M.B., Urdaneta, M. and Ortega, A., 2005, "Experiments and Modeling of the Hydraulic Resistance and Heat Transfer of In-Line Square Pin Fin Heat Sinks with Top By-Pass Flow", *Int. J. Heat Mass Transfer*, Vol. 48, pp. 5058 – 5071.
- Fluent Inc. User's guide, 2006, 6.3.13 version.
- Kim, S.-E. and Choudhury, D., 1995, "A Near-Wall Treatment Using Wall Functions Sensitized to Pressure Gradient", *ASME FED, Separated and Complex Flows*, Vol. 217.
- Launder, B. E. and Spalding, D. B., 1974, "The Numerical Computation of Turbulent Flows", *Computer Methods in Applied Mechanics and Engineering*, Vol. 3, pp. 269-289.
- Mohamed, M.M., 2006, "Air Cooling Characteristics of a Uniform Square Modules Array for Electronic Device Heat Sink", *Applied Thermal Eng.*, Vol. 26, pp. 486 – 493.
- Sahiti, N., Lemouedda, A., Stojkovic, D., Durst, F. and Franz, E., 2006, "Performance Comparison of Pin Fin In-Duct Flow Arrays with Various Pin Cross-Sections", *Applied Thermal Eng.*, Vol. 26, pp. 1176 – 1192.
- Shih, T.-H., Liou, W.W., Shabbir, A., Yang, Z. and Zhu, J., "A New $k-\epsilon$ Eddy-Viscosity Model for High Reynolds Number Turbulent Flows- Model Development and Validation", *Computers Fluids*, Vol. 24, No. 3, pp. 227-238.
- Yang, K.-S., Chiang, C.-M., Lin, Y.-T., Chien, K.-H. and Wang, C.-C., 2007a, "On the Heat Transfer Characteristics of Heat Sinks: Influence of Fin Spacing at Low Reynolds Number Region", *Int. J. Heat Mass Transfer*, Vol. 50, pp. 2667–2674.
- Yang, K.-S., Chu, W.-H., Chen, I.-Y. and Wang, C.-C., 2007b, "A Comparative Study of the Airside Performance of Heat Sinks Having Pin Fin Configurations", *Int. J. Heat Mass Transfer*, Vol. 50, pp. 4661–4667.

9. RESPONSIBILITY NOTICE

The authors are the only responsible for the printed material included in this paper.